Semiquantitative Relationship between Polymer Side-Chain Dynamics and Solvent Solubility Parameters. Variable-Frequency ^{13}C NMR Relaxation Study of Poly(*n*-butyl methacrylate)

George C. Levy* and Dehua Wang†

NIH Research Resource for Multi-Nuclei NMR and Data Processing, Chemistry Department, Syracuse University, Syracuse, New York 13210. *Received May 2, 1985*

ABSTRACT: Extensive ^{13}C NMR relaxation measurements on poly(*n*-butyl methacrylate) (PBMA) obtained at three widely separated frequencies (90.6, 37.8, and 20.0 MHz) show wide variation of spin–lattice relaxation times (T_1s) and nuclear Overhauser effects (NOEs) for the polymer side-chain carbons as a function of the solvent solubility parameter ($\Delta\delta$). A semiquantitative relationship between polymer side-chain motion and the solubility parameters (and therefore cohesive energy) was established. Several sets of spin–lattice relaxation data from the literature have been rationalized by this relationship. The diamond-lattice conformational jump model (VJGM model) has been modified to explain both backbone motion and side-chain multiple internal rotations. The modified model predicts both correlation times for backbone motion and side-chain multiple internal rotations, which can quantitatively reproduce most of the observed data. A heteronuclear 2D NOE (HOESY) experiment was performed to detect dipolar interactions between the quaternary carbon (C-CR_4) and nearby protons. It is found that the NOEs of C-CR_4 mainly come from dipolar interactions with protons of the attached methyl group C-CH_3.

Introduction

^{13}C dipole–dipole spin–lattice relaxation measurements represent a powerful method for investigating dynamics of molecular motion in polymers. Measurements of ^{13}C spin–lattice relaxation times (T_1s), and nuclear Overhauser effects (NOEs) have provided information about backbone motion and segmental internal rotation in synthetic polymers.[1-11] It has been found in several polymers that T_1 values of the backbone chain are unaffected by large changes in macroscopic viscosity from varying molecular weight or concentration in the same solvent.[4] However, the T_1 values do vary with solvent. Heatley and Wood[6] reported the CH_2 proton T_1s for polystyrene in four different solvents. They found that spin–lattice relaxation times in poor solvents were smaller than in good solvents. This implies that segmental motion is hindered in the more tightly coiled conformation adopted in a poor solvent. Similar solvent dependence for main-chain motion has been reported by several other investigators.[7-11] However, little information has been obtained about the dependence of side-chain motion on different solvents, especially in concentrated solutions. Poly(*n*-butyl methacrylate) (PBMA) possesses four protonated carbons in its regular side chain.

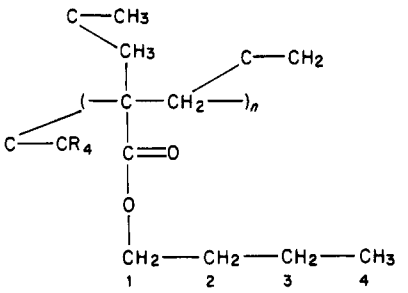

We previously reported an extensive ^{13}C NMR relaxation study of this polymer at a number of temperatures and at two widely different magnetic fields.[5] As a further investigation to include information about the dependence of relaxation on solvents, we have measured spin–lattice relaxation times and NOEs for PBMA in a number of solvents at three dispersed magnetic fields.

A number of models have been developed for interpretation of spin relaxation data. The simplest motional model is rigid isotropic tumbling, characterized by a single correlation time.[12] This model is understandably unable to account for experimental relaxation data for polymers.[4] A second kind of model describes empirical distributions of correlation times. Although Cole–Cole[13] and Fuoss–Kirkwood[14] symmetrical distributions have been used to explain polymer magnetic relaxation, Schaefer's asymmetrical log χ^2 distribution[15] is more proficient. These models have been shown to be consistent with experimental data for many polymers in dilute solution.[4,5,15] However, the physical insight of the empirical distribution models has been questioned,[4] since there is lack of direct connection with specific polymer motions.

The most successful descriptive method to date combines a crankshaft motion and a three-bond jump on a diamond lattice. This latter model was first derived by Valeur, Jarry, Geny, and Monnerie (VJGM).[16-18] The VJGM model, however, only satisfies polymer main-chain motions. It cannot be used to explain side-chain multiple internal rotations. In this paper, a model for polymer motion incorporating side-chain segmental internal rotation will be proposed and applied to the interpretation of ^{13}C spin–lattice relaxation of both main-chain and side-chain carbons in PBMA in concentrated solution.

Experimental Section

Poly(*n*-butyl methacrylate) was purchased from Polyscience, Inc., as a high molecular weight material. Solutions were prepared without further purification using reagent-grade toluene, tetrahydrofuran, acetone, dioxane, aniline, quinoline, 2-propanol, and benzyl alcohol. All samples (476 mg/mL, which is equivalent to 50% (w/w) for PBMA in toluene) were prepared by solute concentration.

Natural abundance ^{13}C spectra were obtained with a quadrature detection-modified Bruker WM-360, in-house design Mohawk-150, and Varian CFT-20 spectrometers, respectively. Free induction decays were accumulated with 4K/4K data points. A fast inversion recovery (FIRFT) pulse sequence[19] with 3-s delay time between repetitions was used. A total of 15 τ values ranging from 0.001 to $5T_1$ s was used to obtain a given T_1 data set. The T_1 values were obtained by using a three-parameter exponential fit and are estimated to be accurate to ±5%. Nuclear Overhauser enhancement factors (NOEFs) were determined with gated decoupling. Two sets of spectra were obtained alternately with two

† Present address: Changchun Institute of Applied Chemistry, China.

0024-9297/86/2219-1013$01.50/0

Table I
T_1 of Poly(n-butyl methacrylate) Carbons in Different Solvents (476 mg/mL) and Different Magnetic Fields at 45 °C

solvent	$\Delta\delta$,[a] $(cal/cm^3)^{1/2}$	T_1, s C-1	C-2	C-3	C-4	C-CH_3	C-CH_2	C-CR_4
				90.6 MHz				
toluene	0.15	0.54	0.55	1.3	2.6	0.087	0.20	2.4
tetrahydrofuran	0.35	0.47	0.60	1.2	2.7	0.086	0.19	2.9
chlorobenzene	0.75	0.43	0.58	1.4	2.7	0.086	0.15	2.4
acetone	1.15	0.46	0.59	1.1	2.5	0.098	0.21	2.8
dioxane	1.25	0.45	0.54	1.0	2.3	0.074	0.20	2.9
aniline	1.55	0.29	0.50	0.90	2.2	0.090	0.25	
quinoline	2.05	0.39	0.47	0.75	2.1	0.078	0.18	3.2
2-propanol	2.75	0.46	0.48	0.80	2.2	0.089		3.5
benzyl alcohol	3.35		0.43	0.75	2.0	0.087	0.23	3.5
average		0.44				0.086	0.20	
				37.8 MHz				
toluene	0.15	0.21	0.50	0.90	1.9	0.047	0.038	1.0
tetrahydrofuran	0.35	0.16	0.58	0.90	1.9	0.026	0.032	1.3
chlorobenzene	0.75	0.29	0.45		1.8	0.027	0.035	1.3
acetone	1.15	0.21	0.49	0.65	1.7	0.040	0.052	0.75
dioxane	1.25	0.25	0.31	0.61	1.7	0.037	0.051	1.0
aniline	1.55	0.29	0.30	0.54	1.7	0.032	0.035	1.4
quinoline	2.05	0.28	0.27	0.60	1.7	0.027		1.8
2-propanol	2.75	0.22	0.32	0.61	1.4	0.040		1.4
benzyl alcohol	3.35		0.25	0.49	1.5	0.045		1.6
average		0.24				0.036	0.041	
				20.0 MHz				
toluene	0.15	0.091	0.28	0.62	1.5	0.038	0.038	0.41
tetrahydrofuran	0.35	0.065	0.27	0.71	1.5	0.039	0.022	0.40
chlorobenzene	0.75	0.071	0.29	0.70	1.4	0.030	0.030	0.47
acetone	1.15	0.092		0.67	1.5	0.044	0.030	0.43
dioxane	1.25	0.075	0.26	0.45	1.6	0.031	0.010	0.42
aniline	1.55	0.079	0.23	0.34	1.1	0.041		0.64
quinoline	2.05	0.10	0.22	0.30	1.1	0.028	0.022	0.72
2-propanol	2.75	0.10	0.30	0.55	1.2	0.041	0.020	0.46
benzyl alcohol	3.35		0.22	0.37	1.1	0.040		0.57
average		0.084				0.037	0.025	

[a] $\Delta\delta$ is the difference of solubility parameters between poly(n-butyl methacrylate) (δ = 8.75 $(cal/cm^3)^{1/2}$) and solvent.

level continuous wideband decoupling and gated decoupling, with a pulse interval greater than 10 times the longest T_1. NOEF values were calculated from the average of the two data sets and were accurate to better than ±15%.

A program for our motional model was written in Fortran 77 with a Simplex nonlinear least-squares optimization algorithm. The calculations for other models were done with our recently developed program MOLDYN,[20] which enables a scientist to explore over 22 molecular motional models. All the calculations were performed on a Data General MV 8000 minicomputer.

The pulse sequence for heteronuclear 2D NOE (HOESY) experiments follows:

$$^1H\ 90°\text{–}t_1/2\text{–}-t_1/2\text{–}90°\text{–}t_2$$

$$^{13}C\ t_1/2\text{–}180°\text{–}t_1/2\text{–}-\tau_m\text{–}90°$$

The 90° pulse width for ^1H was 42 μs. A 16-step phase cycling was used to separate the positive and negative modulation frequencies (hence quadrature detection in F_1), suppress unwanted axial peaks, and cancel the image along $F_1 = 0$. The repetition delay was 0.75 s, which is $1.3T_1$ for the mean proton. Because we are interested in dipolar interactions between quaternary carbons and neighboring protons of methyl groups, the mixing time τ_m was set at 0.49 s, which is equal to T_1 for the methyl group protons. In order to minimize the required acquisition frequency and amount of data-storage space, as well as to optimize decoupling, the proton transmitter frequencies were set to the center of the chemical shift region of interest. Before Fourier transformation, a Gaussian digital filtering function was applied in F_1 and F_2 dimensions, respectively. The spectrum was obtained on a Bruker WM-360 WB spectrometer equipped with an Aspect-2000A computer.

Theory

For two nonequivalent spin $^1/_2$ nuclei the expressions of the spin–lattice relaxation rate $1/T_1$, the spin–spin relaxation rate $1/T_2$, and the nuclear Overhauser enhancement factor were first described by Purcell and co-workers[12]

$$\frac{1}{NT_1} = \frac{2}{15}\frac{\gamma_I^2\gamma_S^2S(S+1)\hbar^2}{r_{IS}^6}[J_0(\omega_I-\omega_S) + 3J_1(\omega_I) + 6J_2(\omega_I+\omega_S)] \quad (1)$$

$$\frac{1}{NT_2} = \frac{1}{15}\frac{\gamma_I^2\gamma_S^2S(S+1)\hbar^2}{r_{IS}^6}[J_0(\omega_I-\omega_S) + 3J_1(\omega_I) + 6J_2(\omega_I+\omega_S) + 4J_0(0) + 6J_1(\omega_S)] \quad (2)$$

$$\mathrm{NOE} = 1 + \frac{\gamma_S}{\gamma_I}\left[\frac{6J_2(\omega_I+\omega_S) - J_0(\omega_I-\omega_S)}{J_0(\omega_I-\omega_S) + 3J_1(\omega_I) + 6J_2(\omega_I+\omega_S)}\right] \quad (3)$$

where r in this case is the carbon–hydrogen internuclear distance, γ_I and γ_S are the magnetogyric ratios of carbon and hydrogen, respectively, N is the number of directly attached hydrogens (for ^{13}C–^1H dipolar relaxation), $J_i(\omega)$ is the spectral density function, which is the Fourier transform of the correlation function

$$J(\omega) = \int_{-\infty}^{\infty} C(t)e^{-i\omega t}\,dt = 2\,\mathrm{Re}\int_0^{\infty} C(t)e^{-i\omega t}\,dt \quad (4)$$

If a molecule undergoes isotropic tumbling, the spectral density function can be described by a single correlation time.

$$J(\omega) = \tau/(1+\omega^2\tau^2) \quad (5)$$

Polymer dynamics, however, is usually too complicated to be assigned to an isotropic motion. Thus a number of dynamic models have been developed. Of many available models the diamond-lattice conformation jump is most realistic. Details of the autocorrelation function and spectral density for this model will now be discussed briefly.

Diamond-Lattice Model. The autocorrelation function for the VJGM model is given by[16-18,21-23]

$$C_{VJGM}(t) = e^{-|t|/\tau_0 + |t|/\tau_d} \operatorname{erfc} (|t|/\tau_d)^{1/2} \quad (6)$$

Two correlation times τ_d and τ_0 are required for description of this model. τ_d characterizes the three-bond conformation jump in an ideal diamond lattice, and τ_0 reflects the long-range tumbling. erfc is the complementary error function.

The spectral density corresponding to eq 6 is[22,23]

$$J(\omega) = \frac{\tau_0\tau_d(\tau_0 - \tau_d)}{(\tau_0 - \tau_d)^2 + \omega^2\tau_0^2\tau_d^2}\left\{\left(\frac{\tau_0}{2\tau_d}\right)^{1/2}\left[\frac{(1 + \omega^2\tau_0^2)^{12} + 1}{1 + \omega^2\tau_0^2}\right]^{1/2} + \left(\frac{\tau_0}{2\tau_d}\right)^{1/2}\frac{\omega\tau_0\tau_d}{\tau_0 - \tau_d}\left[\frac{(1 + \omega^2\tau_0^2)^{1/2} - 1}{1 + \omega^2\tau_0^2}\right]^{1/2} - 1\right\} \quad (7)$$

Polymer Diamond-Lattice Conformation Jump with Side-Chain Internal Rotation. The VJGM model was successfully applied to polymer main-chain motion,[21-23] but it cannot be applied to describe PBMA motion in concentrated solution since both main-chain diffusion and side-chain internal rotation should be considered for this complicated polymer system. We thus modified the VJGM model by superimposing side-chain internal rotation on main-chain motion. We adopted the "model-free" correlation function of internal rotation of a polymer side chain, which has been described by Szabo and Lipari.[24]

$$C_i(t) = S^2 + (1 - S^2)e^{-t/\tau_e} \quad (8)$$

where S^2 ($0 \le S^2 \le 1$) is the degree of spatial restriction of the internal rotation and τ_e is an effective correlation time. If $S^2 = 0$, then the internal motion is similar to isotropic. On the other hand, if $S^2 = 1$, then the internal motion is completely restricted (rigid).

The correlation function for conformational jumps of polymer main chains with internal rotation of side chains can be written as the product of correlation functions for the main-chain motion and that for internal motion, provided that the two motions can be considered independent and uncorrelated.[24-26] If the overall motion is not isotropic, the total correlation function cannot be rigorously factored into a produce of correlation functions of overall and internal motions. Nevertheless, Szabo et al.[24] have shown with convincing evidence that this decoupling approximation is valid for the model of overall anisotropic motion of a main chain with internal rotation of side chain even in cases where a distribution of correlation times has been involved (e.g., for random-coil polymers). We approximate the total correlation function as a product of the diamond-lattice correlation function and internal rotation

$$C(t) = [e^{-|t|/\tau_0 + |t|/\tau_d}][\operatorname{erfc} (|t|/\tau_d)^{1/2}][S^2 + (1 - S^2)e^{-t/\tau_e}] \quad (9)$$

The nuclear spin relaxation parameters are expressed in terms of the spectral density.

$$J(\omega) = \frac{1}{2}\int_{-\infty}^{\infty} C(t)e^{-i\omega t}\,dt = \frac{1}{2}\int_{-\infty}^{\infty}[e^{-|t|/T_0 + |t|/T_d}] \times [\operatorname{erfc} (|t|/T_d)^{1/2}][S^2 + (1 - S^2)e^{-t/\tau}]\,[e^{-i\omega t}]\,dt = \frac{S^2T_0T_d(T_0 - T_d)}{(T_d - T_0)^2 + \omega^2T_0^2T_d^2} \times \left\{\left(\frac{T_0}{2T_d}\right)^{1/2}\left[\frac{(1 + \omega^2T_0^2)^{1/2} + 1}{1 + \omega^2T_0^2}\right]^{1/2} + \left(\frac{T_0}{2T_d}\right)^{1/2}\frac{\omega T_0T_d}{T_0 - T_d}\left[\frac{(1 + \omega^2T_0^2)^{1/2} - 1}{1 + \omega^2T_0^2}\right]^{1/2} - 1\right\} + \frac{(1 - S^2)T_0T_d\tau_e(T_0\tau_e - T_d\tau_e - T_0T_d)}{(T_d\tau_e - T_0\tau_e + T_0T_d)^2 + \omega^2T_0^2T_d^2\tau_e^2} \times \left\{\left(\frac{T_0\tau_e}{2T_d}\right)^{1/2}\left[\frac{[(\tau_e + T_0)^2 + \omega^2\tau_e^2T_0^2]^{1/2} + (\tau_e + T_0)}{(\tau_e + T_0)^2 + \omega^2T_0^2\tau_e^2}\right]^{1/2} + \left(\frac{T_0\tau_e}{2T_d}\right)^{1/2}\frac{\omega T_dT_0\tau_e}{T_0\tau_e - T_d\tau_e - T_0T_d} \times \left[\frac{[(\tau_e + T_0)^2 + \omega^2\tau_e^2T_0^2]^{1/2} + (\tau_e + T_0)}{(\tau_e + T_0)^2 + \omega^2T_0^2\tau_e^2}\right]^{1/2} - 1\right\} \quad (10)$$

There are four parameters in our model. τ_d and τ_0 are correlation times of backbone motion characterized as in eq 6. S^2 and τ_e are the parameters for side-chain internal rotation with physical meaning the same as in eq 8. If there is no side-chain motion in the polymer, then $S^2 = 1$, eq 10 is reduced to eq 7, and the VJGM model is recovered.

To extract dynamic information about side-chain motion, the first step is to evaluate the dynamic parameters τ_d and τ_0 for main-chain motion. For a nucleus in the macromolecular backbone, $S^2 = 1$, the values τ_d and τ_0 can be determined by a nonlinear optimization from multinuclear relaxation experimental data (T_1 and NOE values). After τ_d and τ_0 are fixed, S^2 and τ_e are obtained by the same program from side-chain carbon T_1s and NOEs.

Results and Discussion

The T_1 values of PBMA in three dispersed magnetic fields and in nine selected solvents that have quite varied solubility for PBMA are listed in Table I. This reveals a few interesting trends. The T_1s for the main-chain carbons C-CH_2 generally increase with the strength of magnetic field. This is expected since our measurements were performed in concentrated solutions near room temperature (45 °C), where the main-chain motion should be quite slow (outside of extreme narrowing). One interesting fact that has been observed previously is that the T_1s for all side-chain carbons including the methyl groups also show a consistently large field dependence. Simple theory[27,28] predicts that the dipolar T_1 of a carbon is independent of the magnetic field strength if the correlation time is within the extreme narrowing region.

A few papers have discussed the solvent dependence of T_1 values on polymer main chains.[2,6-11] Generally, in dilute solution (<50 mg/mL) polymer main chains have higher T_1 values in good solvents and lower T_1 values in poor solvents. Our experiment shows that this observation is not seen for concentrated polymer solutions (where $\omega_0^2\tau_c^2$ presumably will always exceed 1 at current magnetic fields,

Table II
NOEF of Poly(*n*-butyl methacrylate) Carbons in Different Solvents (476 mg/mL) and Different Magnetic Fields at 45 °C

solvent	$\Delta\delta$, $(cal/cm^3)^{1/2}$	NOEF						
		C-1	C-2	C-3	C-4	C-CH_3	C-CH_2	C-CR_4
				90.6 MHz				
toluene	0.15	0.97	1.3	1.6	1.9	0.94	0.44	0.72
tetrahydrofuran	0.35	0.83	1.4	1.6	1.7	0.66	0.54	0.63
chlorobenzene	0.75	0.74	1.4	1.6	1.7	1.0	0.39	0.61
acetone	1.15	0.84	1.4	1.5	1.7	0.89	0.47	0.67
dioxane	1.25	0.41	1.3	1.6	1.5	0.73	0.41	0.85
aniline	1.55	0.94	1.1	1.4	1.9	1.0	0.42	0.67
quinoline	2.05	1.0	.78	1.5	1.7	0.94	0.43	0.88
2-propanol	2.75	0.90	1.3	1.5	1.7	0.87		0.87
benzyl alcohol	3.35		1.1	1.6	1.7	0.92	0.35	0.70
average		0.82				0.88	0.39	
				37.8 MHz				
toluene	0.15	0.50	0.94	1.4	1.5	0.96	0.39	0.71
tetrahydrofuran	0.35	0.74	1.1	1.5	1.7	0.88	0.35	0.45
chlorobenzene	0.75	0.71	1.4	1.6	1.7	1.2	0.48	0.48
acetone	1.15	0.65	1.3	1.2	1.3	0.55	0.48	0.45
dioxane	1.25	0.94	0.84	1.1	1.2	0.90		
aniline	1.55	0.95	1.3	1.3	1.5	0.98	0.38	0.65
quinoline	2.05		1.3	1.4	1.7	0.91	0.37	0.74
2-propanol	2.75	0.98	1.1	1.1	1.3	1.0		
benzyl alcohol	3.35		1.1	1.7	193	1.0		0.63
average		0.78				0.93	0.41	
				20.0 MHz				
toluene	0.15	0.67	1.1	1.4	1.2	1.7	0.56	0.84
tetrahydrofuran	0.35	0.92	0.91	1.2	1.2	1.4	0.47	0.79
chlorobenzene	0.75	0.67	1.3	1.7	1.4	1.2	0.45	0.56
acetone	1.15	0.40	1.1	1.3	1.3	1.2	0.55	0.69
dioxane	1.25	0.59				1.4	0.50	
aniline	1.55	1.0	1.0	1.7	1.0	1.5		0.57
quinoline	2.05	0.90	0.92	1.7	1.0	1.6		0.67
2-propanol	2.75	0.76	0.79	1.5	0.94	1.6		0.53
benzyl alcohol	3.35		0.73	1.1	0.98	1.0	0.33	0.57
average		0.73				1.4	0.48	

at least for vinyl polymers with side chains such as PBMA).[38] As Table I indicates, the T_1 values of C-CH_2 remain relatively constant over the wide solvent range studied at a concentrated solution (476 mg/mL, equivalent to 50% (w/w) of PBMA in toluene). Recent studies indicate that the relaxation of polymer main chains arises mainly from short-range chain conformation jumps and long-range chain overall tumbling.[4,21-23] A shallow minimum had been observed for PBMA in the original variable-temperature experiments.[5] However, we have not observed any shallow minimum by changing solvents in the current study. In fact, as shown below, backbone CH_2 carbon NOEF values are similar in all solvents, and this lack of dependence can be used to infer relative solvent insensitivity of τ_c, giving justification to the use of average T_1s and NOEs for the calculation of backbone motional parameters. (We thank one of our reviewers for suggesting we include this point.) The T_1s for the side-chain carbons increase as a function of distance from the main chain, as observed in the earlier paper.[5]

The most fruitful experimental result observed in this paper is the relationship between the T_1s of side-chain carbons and the thermodynamic property, cohesive energy, of polymer and solvent. Each molecule in a liquid or solid possesses potential energy due to van der Waals attraction forces. The potential energy of 1 cm^3 of material is defined as the cohesive energy density.[29] The square root of the cohesive energy density is termed as the solubility parameter, δ. The cohesive energy is actually related to the intensity of intermolecular interactions; therefore, it relates with many physical properties such as ultimate strength, compressibility, thermal expansion coefficient, and so on. Cohesive energy has also been used to predict the solubility and solvent sensitivity of polymers. The closer the solubility parameter of solvent to that of the polymer, the better the solvent for that polymer, $\Delta\delta$ is the difference of solubility parameters between polymer and solvent. As shown in Table I, an increase in $\Delta\delta$ results in a decrease in side-chain T_1 values. This is evidence that the side-chain motion is affected by intermolecular interaction between polymer and solvent. These interactions increase as a function of distance from the main chain.

Table II lists the nuclear Overhauser enhancement factors for PBMA. The NOEFs of side-chain carbons C-2, C-3, and C-4 show some tendency to decrease as a function of $\Delta\delta$ NOEF of main-chain carbon C-CH_2 remains relatively constant except possibly at 20 MHz over the solvent range studied. C-CH_3 and C-1 are anchored at the main chain or are very close to main chain; their NOEF values have similar behavior as does the backbone chain.

An interesting experimental observation is the different trends of NOEF magnetic field dependence betwen the main-chain carbon and side-chain carbons. The NOEF values of backbone carbon C-CH_2 increases with decreasing magnetic field. However, the NOEF values of side-chain carbons C-1–C-4 decrease with decreasing magnetic field. This is an atypical magnetic field dependence of NOEF and is explained later by our model.

Main-Chain Carbons. Table III lists the calculated ^{13}C relaxation parameters for the main-chain methylene carbon by our model, the model-free approach,[24] and log χ^2 model.[15] All three models can be fit quite well to the T_1s and NOEFs obtained at three magnetic fields. However, it is significant to observe which model gives the most reasonable and physically meaningful results. Table IV gives the molecular dynamics parameters resulting from these calculations. The correlation time τ_d for three-bond conformation jump and τ_0 for long-range chain tumbling

Table III
Calculated ^{13}C Relaxation Parameters for C-CH_2, C-1, and C-CH_3 of Poly(*n*-butyl methacrylate)

		exptl data[a]		calcd data: present model		calcd data: model free		calcd data: log χ^2	
	magnetic field, MHz	NT_1, s	NOE	NT_1, s	NOE	NT_1, s	NOE	NT_1, s	NOE
C-CH_2	90.6	0.40	1.4	0.33	1.4	0.35	1.4	0.33	1.3
	67.9	0.22	1.3	0.22	1.4	0.22	1.3	0.23	1.3
	37.8	0.082	1.4	0.099	1.4	0.093	1.3	0.12	1.4
	20.0	0.050	1.5	0.041	1.4	0.047	1.4	0.059	1.5
C-1	90.6	0.88	1.8	0.95	2.0	0.92	2.0		
	37.8	0.48	1.8	0.40	1.7	0.35	1.6		
	20.0	0.17	1.7	0.18	1.6	0.19	1.6		
C-CH_3	90.6	0.26	1.9	0.26	2.5	0.25	1.8		
	37.8	0.11	1.9	0.13	1.9	0.12	2.2		
	20.0	0.11	2.4	0.067	1.6	0.089	2.3		

[a] The experimental NT_1 and NOE are the average values from 9 different solvents.

Table IV
Calculated Dynamic Parameters[a] of C-CH_2, C-1, and C-CH_3 of Poly(*n*-butyl methacrylate)

	present model		model-free approach			log χ^2	
	T_d, s	T_0, s	A	τ_1, s	τ_2, s	τ, s	p
C-CH_2	1.1×10^{-8}	4.2×10^{-8}	0.67	5.4×10^{-9}	4.1×10^{-11}	1.0×10^{-8}	8

	present model		model-free approach	
	S^2	τ_e, s	S^2	τ_e, s
C-1	0.21	2.5×10^{-11}	0.22	3.2×10^{-11}
C-CH_3	0.53	2.3×10^{-10}	0.21	7.3×10^{-10}

[a] Parameters described in the text and ref 24 (model-free approach) and ref 15 (log $-\chi^2$ model).

(our model) are calculated to be 1.1×10^{-8} and 4.2×10^{-8} s, respectively. The log χ^2 gives similar results for its effective correlation time, 1.0×10^{-8} s, and width parameter, $p = 8$, which corresponds to a reasonally wide distribution. Both of the models indicate that the correlation time for main-chain motion is located at a shallow minimum in a T_1 plot with respect to correlation time. The virtual insensitivity of the experimental main-chain T_1 values to change in solvent indicates that a value near 10^{-8} s is reasonable for the correlation time for a slow main-chain motion in concentrated solution. The calculated correlation times from the model-free approach are 5.4×10^{-9} and 4.1×10^{-11} s and $A = 0.67$ (ref 24 gave similar values). These values are probably too small for the correlation times of main-chain motion in such concentrated solutions of PBMA. The model-free approach combines main-chain anisotropic overall motion with side-chain internal rotation. The overall motion, characterized by three adjustable parameters A, τ_1, and τ_2 (see ref 24 for details), might not be compatible with the complicated motion of PBMA. It may be one reason why this model gives unrealistically small correlation times for backbone motion. (On the other hand it is only fair to point out that for C-CH_2 NOEs, the model-free approach gives a better fit to the experimental data).

C-CH_3 Carbons. C-CH_3 is the methyl group directly attached to the backbone. The T_1s and NOEs of these methyl groups show trends indistinguishable from those observed for the main-chain methylene carbons. T_1s and NOEs remain relatively constant over a wide range of solvents; a decrease in magnetic fields leads to some decrease in T_1 values and an increase in NOEs. Our model combines Szabo's internal rotation model[24] with the VJGM diamond-lattice conformation jump model.[16-18] The degree of spatial restriction S and the effective correlation time τ_e are shown in Table IV. The effective correlation time calculated by our model (2.3×10^{-10} s) is 3 times smaller than that calculated by the model-free approach (7.3×10^{-10} s). Moreover the degree of spatial restriction of the methyl group calculated by the model-free approach, 0.21, is much lower than that calculated by our model (0.53). Note that the model-free approach gives almost the same spacial restriction values for C-CH_3 (0.21) and C-1 (0.22), whereas our model shows that the spatial restriction of C-CH_3 (0.53) is considerably higher than, that of C-1 (0.21). The value given by our model seems more reasonable since C-1 is connected through oxygen and is three bonds away from the backbone, whereas C-CH_3 is directly anchored at the main chain.

C-1 Carbons. As shown in Table II a decrease in magnetic field leads to a decrease in NOEF of C-1 and other side-chain carbons. The simple isotropic model with a single-exponential correlation time is unable to account for this fact, since it predicts that the NOEF increases or remains constant (in the extreme narrowing region) with decrease of the magnetic field. This complex behavior observed in nuclear Overhauser enhancement experiments arises from the juxtaposition of various motions over a wide range of time scales. The polymer side chain undergoes at least two kinds of motions: overall tumbling and internal rotation. Our model has considered the internal rotation superimposed upon the overall molecular motion. Figure 1 illustrates a theoretical NOEF curve calculated from our model. As the correlation times increase from 8×10^{-12} s the expected NOEF starts to deviate for the two magnetic field strengths. The NOEF at low field is greater than that in high field. As correlation times become longer than 10^{-9} to 10^{-8} s, the NOEF at high field starts to get greater. The experimental NOEF data (Table II) verify this theoretical prediction qualitatively. The dynamic parameters for our model and the model-free approach are listed in Table IV. The spatial restriction for carbon C-1 is 0.21, and the effective correlation time is 2.5×10^{-11} s, which is the point in Figure 1 to have an abnormal field dependent NOEF.

C-2–C-4 Carbons. Previous research has shown that the T_1 values of main-chain carbons remain relatively constant with large changes in macroscopic viscosity arising

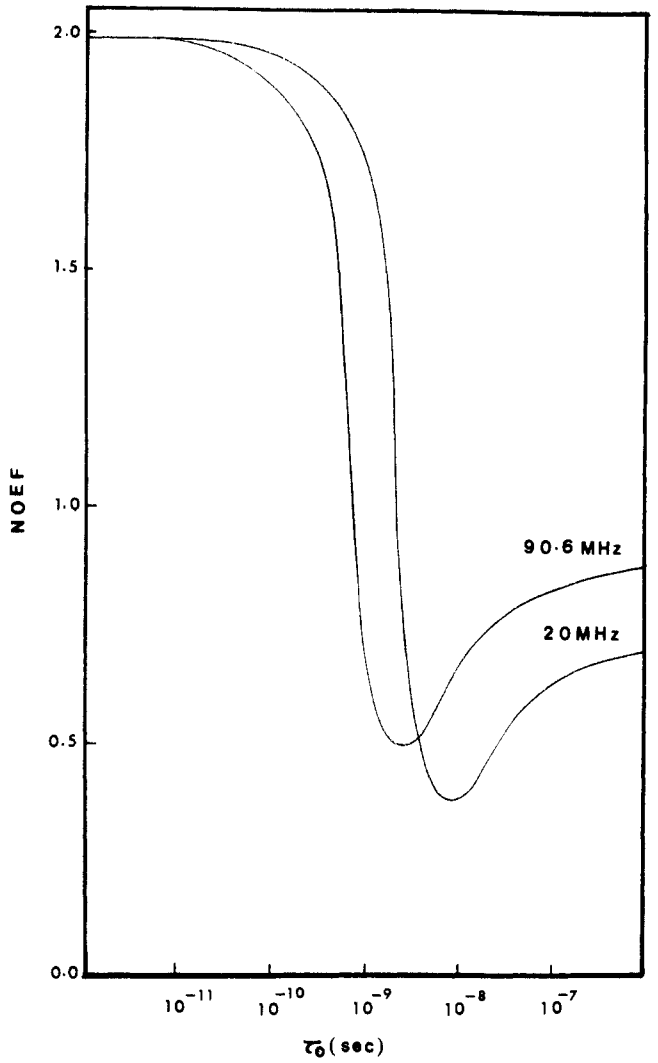

Figure 1. Nuclear Overhauser enhancement factors for C-1 carbon undergoing internal rotation ($S^2 = 0.2$, $\tau_0 = 1.0 \times 10^{-11}$ s) as a functiona of the correlation time of main-chain overall tumbling τ_0 ($\tau_d = 1.0 \times 10^{-8}$ s) at 20 and 90.6 MHz.

Table V
Kinematic Viscosities of Poly(*n*-butyl methacrylate) in Different Solvents (476 mg/mL) at 45 °C

solvent	$\Delta\delta$, $(cal/cm^3)^{1/2}$	viscosity, cSt
toluene	0.15	5682
tetrahydrofuran	0.35	3714
chlorobenzene	0.75	3010
acetone	1.15	31564
dioxane	1.25	3690
aniline	1.55	4127
quinoline	2.05	777
2-propanol	2.75	381681
benzyl alcohol	3.35	6143

from molecular weight or concentration in the same solvent.[4] Our experiments show that these T_1 values are also unaffected by large changes in viscosity arising from varying solvents at the same concentration. As Table I has indicated, the T_1 values of main-chain carbons do not systematically change with solvent, but the side-chain carbon T_1s decrease as a function of $\Delta\delta$.

To verify that the decrease is not due to varying viscosity, the kinematic viscosities of PBMA in different solvents were measured at the same concentration (476 mg/mL) and temperature (45 °C). Table V shows that there is no apparent relation between viscosity and $\Delta\delta$. Therefore there is no apparent relation between the

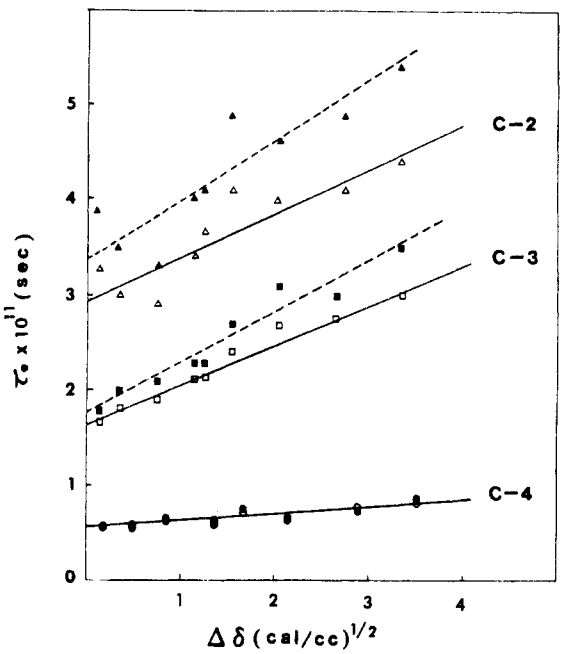

Figure 2. Effective correlation times vs. $\Delta\delta$ for side-chain carbons C-2 (triangles), C-3 (squares), and C-4 (circles) at 45 °C. Data were extracted from the model-free approach (solid symbols) and our model (empty symbols).

side-chain carbon T_1 values and viscosity as indicated in Table I. The measurable decrease in T_1 for side-chain carbons with increasing $\Delta\delta$ implies that intermolecular interactions restrict side-chain spin relaxation in poor solvents.

Figure 2 shows the correlation times increase considerably along the side chain. This is not unexpected, since a similar result has been obtained by previous study.[5,24] The most exciting result is the relationship between the effective correlation time and the thermodynamic parameter, cohesive energy, or its square root, solubility parameter. The effective correlation time increases approximately as a linear function of $\Delta\delta$. The closed symbols were extracted by the model-free approach, and the empty symbols were obtained with our model.

Another feature of Figure 2 is the difference of the calculated correlation times from the two different models for carbon C-2 and C-3, whereas the C-4 carbon (a methyl group at the far end from backbone) shows essentially identical correlation times by the model-free approach and our model. One reason that the C-4 group has a very small spatial restriction (0.0058 for average) is the high symmetry of the methyl groups to internal rotation.

S^2 has been referred to as a spatial restriction. We can see from Figure 3 that the spatial restriction of internal rotation drastically decreases along the chain. On the other hand, S^2 considerably decreases with increasing $\Delta\delta$ until $\Delta\delta$ reaches ~ 2 and then S^2 remains relatively constant. Since as $\Delta\delta$ increases the the solvent becomes poorer for the polymer, the increase in spatial restriction with increase in $\Delta\delta$ indicates that the side chains have high barriers to rotation in poor solvents (vide supra).

From these analyses we can anticipate that the effective correlation time of polymer side-chain carbons may be a good measure of the intensity of intermolecular entanglements. The value $\Delta\delta$ should be able to predict relaxation parameters and dynamics of both main-chain and side-chain carbons in dilute solution. For example, several investigators[6,8,9] have investigated the solvent dependence of relaxation times in dilute solution, although none of those reports discussed the solubility parameter.

Table VI
Diamond-Lattice Correlation Times, Activation Energies, and $\Delta\delta$ from ^1H Relaxation of Polystyrene

solvent	T_1,[a] s	$\tau \times 10^{10}$, s (at 30 °C)	E_a, kJ/mol	$\Delta\delta$, (cal/cm^3)$^{1/2}$
deuteriochloroform	0.90	6	19	0.2
carbon tetrachloride	0.38	16	25	0.5
hexachlorobutadiene	0.30	47	29	0.9

[a] T_1 values were estimated from Figure 4 of ref 3.

We can rationalize the literature data with the concept of $\Delta\delta$. For example, using ^{13}C relaxation experiments, Inoue and Konno[9] found that polystyrene in toluene is more mobile (T_1 longer) than in cyclohexane-$d_{1,2}$. The solubility parameter of polystyrene is 9.1,[29] and $\Delta\delta$ of toluene is 0.2, which is smaller than $\Delta\delta$ for cyclohexane (0.9). Gronski and Murayama[8] also studied the solvent dependence of relaxation times of polystyrene by ^{13}C NMR, and found that the T_1s of the polymer chain are longer in tetrahydrofuran-$d_{1,2}$ than in dioxane. Correspondingly, $\Delta\delta$ of tetrahydrofuran (0.8) is smaller than that of dioxane (1.0).

Proton relaxation can also be used to measure polymer chain mobility. Heatley and Wood[6] measured the CH_2 proton T_1 of polystyrene in three solvents and calculated the correlation times of the main chain with the VJGM model and found the activation energy. The results are listed in Table VI, to which we have added the term $\Delta\delta$. The T_1 values of the CH_2 carbons decrease, and activation energy increases with increasing AK. The AK values of the first two solvents were taken from ref 29 but $\Delta\delta$ for hexachlorobutadiene can not be found in handbooks. We calculated this quantity from the boiling point of hexachlorobutadiene (260.76 °C) and its density (1.665 g/cm^3) according to following equations:[29,30]

$$\delta^2 = (\Delta H_v - RT)/V \quad (11)$$

$$\Delta H_v = 21 T_{bp} \text{ (cal/mol)} \quad (12)$$

$$V = M/d \quad (13)$$

where ΔH_v is the heat of vaporization per mole, R is the gas constant, T is the absolute temperature, T_{bp} is the absolute temperature of the boiling point, V is the molar volume of the solvent, M is the molecular weight, and d is the density.

Caution should be taken when proton relaxation parameters are dealt with, especially when a strong hydrogen bonding compound is used as a solvent, since proton dipolar relaxation could arise from intermolecular relaxation between solute and solute or solute and solvent protons.[31]

The concept of cohesive energy density or a solubility parameter has been used for predicting many polymer properties. In this paper we have extended this concept to predict NMR relaxation parameters and polymer dynamics in solution. Some discrepancies between predictions based on the cohesive energy and experimental results could be possible if the van der Waals potential energy between the polymer and solvent is not the main source of intermolecular interactions. For example, strong hydrogen bonding or chemical reaction could affect the prediction.

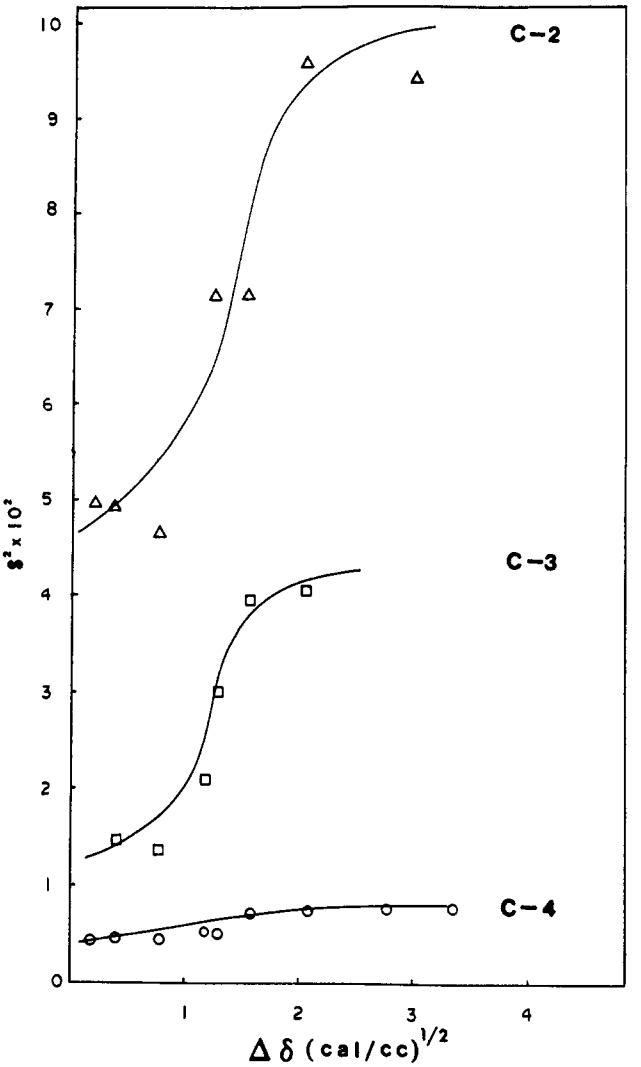

Figure 3. Spatial restriction, S^2, of C-2, C-3, and C-4 as a function of $\Delta\delta$ at 45 °C, extracted from our model.

C-CR$_4$. Relaxation of protonated ^{13}C nuclei in polymers, such as C-CH_2, are dominated by the dipole–dipole mechanism.[5] Since dipolar interactions are related to $(r_{CH})^{-6}$, where r_{CH} is the internuclear distance between carbon and hydrogen, the relaxation rate $1/T_1$ and NOEF of protonated carbons are governed by the attached pro-

Table VII
Degree of Spatial Restriction and Correlation Times of PBMA Side-Chain Internal Rotation in Different Solvents (476 mg/mL) at 45 °C

solvent	$\Delta\delta$, (cal/cm^3)$^{1/2}$	S			$\tau_e \times 10^{11}$, s		
		C-2	C-3	C-4	C-2	C-3	C-4
toluene	0.15	0.050	0.019	0.0045	3.3	1.7	0.57
tetrahydrofuran	0.35	0.050	0.015	0.0045	3.0	1.8	0.56
chlorobenzene	0.75	0.047	0.014	0.0047	2.9	2.8	0.59
acetone	1.15	0.043	0.021	0.0050	3.4	2.1	0.59
dioxane	1.25	0.077	0.030	0.0050	3.5	2.1	0.59
aniline	1.55	0.072	0.040	0.0069	4.1	2.4	0.63
quinoline	2.05	0.096	0.041	0.0065	4.0	2.7	0.66
2-propanol	2.75	0.061	0.021	0.0076	4.1	2.7	0.66
benzyl alcohol	3.35	0.094	0.033	0.0075	4.4	3.0	0.68

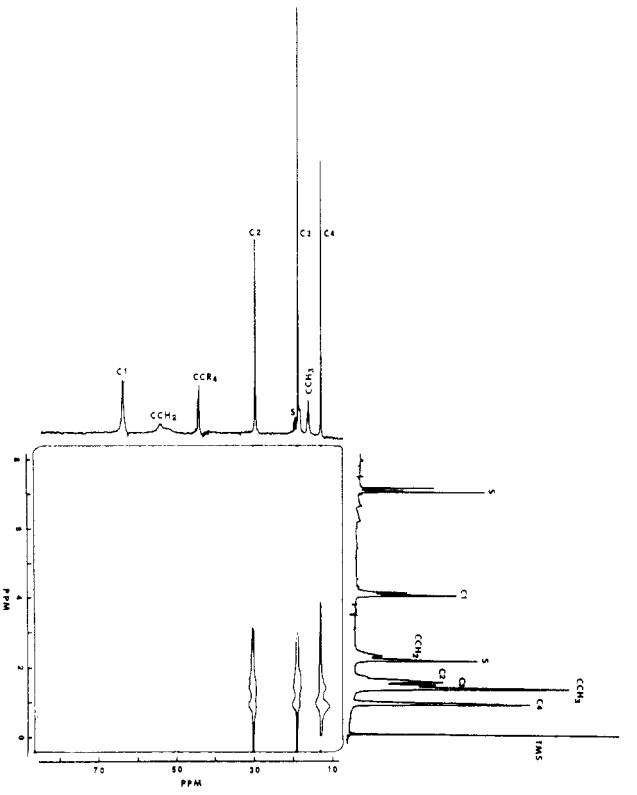

Figure 4. Contour plot of the heteronuclear 2D NOE (HOESY) spectrum of 476 mg/mL poly(*n*-butyl methacrylate) in toluene-d_8. Spectral acquisition parameters: 42-and 13-μs 90° pulses for ^1H and ^{13}C, respectively; 0.073-s acquisition time; 7042-Hz sweep width in the ^{13}C dimension; 0.39-s mixing time; 0.49-s preparation time. Sixty-four spectra (256 scans each) were accumulated with t_1 (158 μs) increased to provide the equivalent of a 1582-Hz sweep width in the ^1H frequency dimension. Zero-filling in the ^1H dimension was executed once (to 128) along the F_1 dimension to make it contain 128 points. Conventional one-dimensional ^{13}C and ^1H spectra are shown along their respective dimensions.

tons. The quaternary carbon (C-CR_4) has no directly attached proton, therefore, dipolar spin relaxation must arise from nearby protons. The previous paper published by our group in 1978 has shown the similarity of temperature and magnetic field dependence between C-CH_2 and C-CR_4 carbons.[5] Thus, the relaxation mechanism for the quaternary carbon C-CR_4 should be dominated (at low or moderate magnetic field) by dipolar interactions, at least in this special example. Quaternary carbon relaxation, however, is difficult to investigate in polymers since there is ambiguity as to dipolar contributions. A recently developed heteronuclear 2D NOE (HOESY) experiment[32-34] is able to elucidate dipolar interactions between an observed nucleus such as ^{13}C or phosphorus and a decoupled nucleus such as ^1H. This technique is especially useful to analyze dipolar relaxation behavior of the quaternary carbon atoms.[33] Furthermore, if the HOESY technique is combined with observed nuclear relaxation data, it should prove useful for evaluation of molecular structure and conformation.

Figure 4 shows the contour plot of the HOESY experiment on 476 mg/mL of poly(*n*-butyl methacrylate). The normal one-dimensional ^{13}C and ^1H spectra are also shown. All of the cross peaks in Figure 4 originate from heteronuclear dipolar interactions. As shown in Figure 4, the dipolar interactions for protonated carbons are strong, hence cross peaks are observed at the intersection of ^1H and ^{13}C chemical shifts. Levy et al.[32,33] found that the NOEs of quaternary carbons mainly come from dipolar interactions with protons of directly attached methyl groups. A similar NOE phenomenon was observed in our HOESY experiment. Figure 4 shows the signals from NOEs to quaternary carbon C-CR_4. The dipolar interactions mainly come from the attached methyl group. No cross peak between the quaternary carbon and the CH_2 protons was observed (partially this may be due to the low intensity of the CH_2 peak).

The proton spectrum of PBMA was not definitively assigned before this work. The HOESY experiment can be applied for this purpose. The full assignment for the ^1H spectrum of PBMA is shown in the F_1 dimension of Figure 4. To confirm the assignment, a heteronuclear chemical shift correlated spectrum was performed. This technique is useful for the assignment of an ^1H spectrum from a known ^{13}C spectrum (or vice versa) since resonances at frequencies $F1$ and $F2$ are connected by heteronuclear scalar spin–spin coupling.[35-37]

Acknowledgment. This work was supported by NSF Grant CHE 81-015109. All NMR spectra were obtained at the NIH Biomedical Technology Research Resource for Multi-Nuclei NMR and Data Processing, NIH Grant RR-01317.

Registry No. Poly(*n*-butyl methacrylate) (homopolymer), 9003-63-8.

References and Notes

(1) (a) Levy, G. C. *J. Am. Chem. Soc.* **1973**, *95*, 6117. (b) Levy, G. C.; Rinaldi, P. L.; Dechter, J. J.; Axelson, D. E.; Mandelkern, L. *ACS Symp. Ser.* **1980**, *No. 142*, 119.
(2) Bovey, F. A.; Jelinski, L. W. *J. Phys. Chem.* **1985**, *89*, 571.
(3) Henrichs, P. M. *J. Polym. Sci.* **1983**, *21*, 263.
(4) Heatley, F. *Prog. Nucl. Magn. Reson. Spectrosc.* **1979**, *13*, 47–85.
(5) Levy, G. C.; Axelson, D. E.; Schwartz, R.; Hochmann, J. *J. Am. Chem. Soc.* **1978**, *100*, 410.
(6) Heatley, F.; Wood, B. *Polymer* **1978**, *19*, 1405.
(7) Heatley, F.; Begum, A. *Makromol. Chem.* **1977**, *178*, 1205.
(8) Gronski, W.; Murayama, N. *Makromol. Chem.* **1978**, *179*, 1609.
(9) Inoue, Y.; Konno, T. *Polym. J. (Tokyo)* **1976**, *8*, 457.
(10) Matsuo, K.; Kuhlmann, K. F.; Yang, H. W.-H.; Geny, F.; Stockmayer, W. H.; Jones, A. A. *J. Polym. Sci., Polym. Phys. Ed.* **1977**, *15*, 1347.
(11) Liu, K.-J.; Anderson, J. E. *Macromolecules* **1970**, *3*, 163.
(12) Bloembergen, N.; Purcell, E. M.; Pound, R. V. *Phys. Rev.*, **1948**, *73*, 679.
(13) Cole, K. S.; Cole, R. H. *J. Chem. Phys.* **1941**, *9*, 341.
(14) Fuoss, R. M.; Kirkwood, J. G. *J. Am. Chem. Soc.* **1941**, *63*, 385.
(15) Schaefer, J. *Macromolecules* **1973**, *6*, 882.
(16) Valeur, B.; Jarry, J. P.; Geny, F.; Monnerie, L. *J. Polym. Sci., Polym. Phys. Ed.* **1975**, *13*, 667.
(17) Valeur, B.; Monnerie, L.; Jarry, J.-P. *J. Polym. Sci., Polym. Phys. Ed.* **1975**, *13*, 675.
(18) Valeur, B.; Jarry, J.-P.; Geny, F.; Monnerie, L. *J. Polym. Phys.* **1975**, *13*, 2251.
(19) Levy, G. C.; Lichter, R. L.; Nelson, G. L. "Carbon-13 Nuclear Magnetic Resonance"; Wiley-Interscience: New York, 1980; Chapter 8.
(20) Craik, D. J.; Kumar, A.; Levy, G. C. *J. Chem. Inf. Comput. Sci.* **1983**, *23*, 30; released through QCPE, 1985.
(21) Skolnick, J.; Yaris, R. *Macromolecules* **1982**, *15*, 1064.
(22) Bendler, J. T.; Yaris, R. *Macromolecules* **1978**, *11*, 650.
(23) Jones, A. A.; Robinson, G. L., Gerr, F. F. *ACS Symp. Ser.* **1979**, *No. 103*, 271.
(24) Lipari, G.; Szabo, A. *J. Am. Chem. Soc.* **1982**, *104*, 4546.
(25) Wallach, D. *J. Chem. Phys.* **1967**, *47*, 5258.
(26) Levy, G. C.; Kumar, A.; Wang, D. *J. Am. Chem. Soc.* **1983**, *105*, 1026.
(27) Abragam, A. "The Principles of Nuclear Magnetism"; Oxford University Press: London, 1961; Chapter 8.
(28) Farrar, T. C.; Becker, E. D. "Pulse and Fourier Transform NMR"; Academic Press: New York, 1971.
(29) Gardon, J. L. In "Encyclopedia of Polymer Science and Technology"; Interscience: New York, 1965; Vol. 3, p 833.
(30) Riddick, J. A.; Bunger, W. B. "Organic Solvents", 3rd ed.; Wiley-Interscience: New York, 1970; p 38.
(31) Levy, G. C.; Wang, D. unpublished data.
(32) Yu, C.; Levy, G. C. *J. Am. Chem. Soc.* **1983**, *105*, 6995.
(33) Yu, C.; Levy, G. C. *J. Am. Chem. Soc.* **1984**, *106*, 6533.

(34) Rinaldi, P. L. J. Am. Chem. Soc. 1983, 105, 5165.
(35) Benn, R.; Günther, H., Angew. Chem., Int. Ed. Engl. 1983, 22, 350.
(36) Maudsley, A. A.; Muller, L.; Ernst, R. R. J. Magn. Reson. 1977, 28, 463.
(37) Bodenhausen, G.; Freemen, R. J. Magn. Reson. 1977, 28, 471.
(38) It should be noted that the definition of τ_c itself may be ambiguous. In any event, for this structural class of polymers, overall polymer motion in these concentrated solutions is slow relative to ω_0.

Poly(vinyl acetate) Dynamics Studied by Proton and Carbon-13 Nuclear Magnetic Resonance in the Solid State

S. Ganapathy,† V. P. Chacko,‡ and R. G. Bryant*†

Departments of Radiology, Biophysics, and Chemistry, University of Rochester, Rochester, New York 14642, and Department of Radiology, Johns Hopkins Medical Center, Baltimore, Maryland 21025. *Received October 7, 1985*

ABSTRACT: Carbon and proton nuclear magnetic resonance measurements have been applied to the poly(vinyl acetate) system in the presence and absence of water. Proton magnetic relaxation dispersion measurements from 0.01 to 30 MHz demonstrate a low-frequency dispersion that indicates a distribution of low-frequency motions that drive the proton magnetic relaxation. The static carbon spectra demonstrate that the carboxyl side-chain region of the polymer is largely unaffected by the addition of water. However, there are dramatic changes in the carbon spin–lattice relaxation rates when the polymer is hydrated. In the presence of water the carbon spin–lattice relaxation is dominated by the high-frequency motion of the water molecules, but carbon relaxation and proton relaxation in the rotating frame are controlled by slower polymer motions of sufficiently small amplitude that the carboxyl carbon chemical shift tensor is largely unaffected.

Introduction

The interaction between water molecules and motions in macromolecular systems is important for understanding materials properties, and in the case of biological catalysts, the details of function and mechanism. Biologically critical molecules such as enzyme catalysts are difficult to study because the considerable monomer heterogeneity produces very complex spectra; simpler polymeric systems may, therefore, serve as reasonable model systems for deducing main dynamical principles, but which are of considerable interest in their own right. The present report concerns the dynamical response of a polymer to the addition of water. Poly(vinyl acetate) was chosen as a model system because of its convenient spectroscopic and physical properties. The monomeric unit is shown in Figure 1.

Motions in polymeric solids have been studied by magnetic resonance methods for a number of years using highly sensitive proton magnetic resonance methods. Attempts are often made to relate the physical properties of the polymer to the proton spin–lattice relaxation times in the laboratory and rotating frames, T_1^H and $T_{1\rho}^H$. A major difficulty with detailed interpretation of proton spin parameters arises because of efficient spin–spin communication between protons in different regions of the polymer, i.e., spin diffusion, which often averages the effects of local dynamical heterogeneity. Nevertheless, such studies have shown clearly that at temperatures below the glass transition temperature, T_g, local motions such as side-chain motions, terminal group rotations, or main-chain local fluctuations dominate the observed nuclear magnetic relaxation behavior, but at temperatures above T_g, backbone motions contribute importantly.[1,2]

It is well-known that the addition of solvent or plasticizer to a glassy polymer lowers T_g, changes the mechanical properties, and is a function of the particular polymer–plasticizer interaction.[3-7] Though there have been a number of NMR studies on polymer dynamics, there have been relatively few that examine the dynamical effects of polymer–solvent interactions. The emergence of high-resolution rare-spin magnetic resonance methods in solids such as cross-polarization[8] magic angle sample spinning[9,10] (CP–MASS) combined with strong dipolar decoupling[11] permits observation of particular monomer carbon resonances, thus providing the possibility of site-specific resolution in an analysis of the polymer dynamics.[12] In glassy polymers there is some broadening of the polymer carbon spectrum obtained under magic angle spinning conditions;[12] however, the resolution is sufficient to resolve all four carbon resonances in poly(vinyl acetate), permitting independent measurement of relaxation rates and in some cases line shapes in nonspinning samples. Since the rare spin is not subject to the relaxation averaging associated with efficient spin diffusion, the carbon spectrum offers site-resolved nuclear magnetic relaxation times. The main parameters that are available include the carbon-13 line shape, the proton relaxation times T_1^H and $T_{1\rho}^H$, and the carbon relaxation times T_1^C and $T_{1\rho}^C$, all sampling somewhat different spectral densities, thus permitting a dynamical characterization that reflects motions at different frequencies.

Earlier work on poly(vinyl acetate) using high-resolution solution-phase NMR methods has shown that water is a poor solvent;[6] however, saturation of the polymer with water lowers the glass transition temperature by 25 °C. Further, it was shown that high-resolution carbon NMR spectra could be obtained at temperatures about 100 °C above T_g using radio-frequency (rf) levels appropriate to scalar decoupling of the protons; however, detailed analysis of polymer motions and the contributions of water were not reported. Here we report an extensive data set on both wetted and dry polymer. We address the contribution of water to both the carbon and proton magnetic relaxation in wetted poly(vinyl acetate) and use the carbon line shape, the carbon relaxation times T_1^C and $T_{1\rho}^C$, and the field dependence of the proton relaxation time T_1^H to partially characterize the motions in the system.

† University of Rochester.
‡ Johns Hopkins Medical Center.

0024-9297/86/2219-1021$01.50/0